ChemComm

Accepted Manuscript

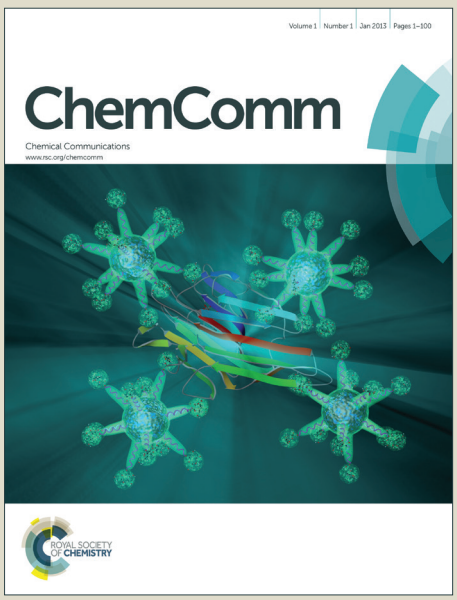

ROYAL SOCIETY OF CHEMISTRY

www.rsc.org/chemcomm

Chem.Comm

RSCPublishing

COMMUNICATION

Synergistically enhanced oxygen reduction activity of MnO_x-CeO_2/ketjenblack composite

Cite this: DOI: 10.1039/xoxxoooooox

Jiajie Chen,[a] Nan Zhou,[b] Haiyan Wang,[a,c,*] Zhiguang Peng,[a] Huiyong Li,[b] Yougen Tang[a,*] and Kun Liu[a]

Received ooth January 2012,
Accepted ooth January 2012

DOI: 10.1039/xoxxoooooox

www.rsc.org/

Here we report a hybrid of MnO_x-CeO_2/ketjenblack as a novel catalyst for oxygen reduction reaction (ORR) by a facile strategy. This hybrid exhibits a comparable activity and better stability towards ORR than the commercial 20wt.% Pt/C due to the synergistic effect.

Oxygen reduction reaction (ORR) plays an important role in electrochemical energy storage and conversion devices such as fuel cells and metal-air batteries.[1, 2] Platinum (Pt) and its alloys are considered as the most efficient catalysts for ORR to date, but their prohibitive cost, scarcity and insufficient durability hinder their successful implementation of these promising technologies.[3] Therefore, it is highly desirable and still challenging to develop non-precious metal ORR catalysts having comparable catalytic performances with the Pt-based materials but with higher stability and much lower cost. Among non-precious metal alternatives, manganese oxides (MnO_x) have attracted tremendous attention because of their low cost, considerable catalytic activity and environmental compatibility. The rich oxidation states, chemical compositions and crystal structures of MnO_x make them one group of promising ORR catalysts in alkaline solution.[4-6] However, MnO_x alone does not catalyze oxygen reduction efficiently probably owing to their low intrinsic electrical conductivity and poor oxygen adsorption capability.[7, 8] Traditionally strategies to enhance the electrocatalytic performance of MnO_x include coating on carbon supports, doping metals ions and introducing oxygen vacancies.[7-11] Despite the fact that these efforts have been proven effectively, the ORR catalytic performance of MnO_x-based materials is still inferior to the state-of-the-art Pt/C catalyst. In addition, the stability of MnO_x still remains a problem caused by different degradation mechanisms during long-term electrochemical operation.[12]

Cerium oxide (CeO_2) is known to be an excellent promoter or support in various catalytic process, especially for the elimination of toxic exhaust gases (CO, SO_2 and NO_x) due to its very unique oxygen storage capability and oxygen transfer ability.[13-15] These unique properties of the CeO_2 also offer a chance to apply its advantages to enhance the ORR catalytic process of MnO_x in alkaline solution. In our recent work, $Mn_{0.3}Ce_{0.7}O_2$ nanoparticulates has been reported, whose electrocatalytic performance towards ORR at high current densities is significantly improved due to the introducing of CeO_2.[16] Generally, the adsorption of oxygen and formation of peroxide have been viewed as initial and the rate-determining ORR steps.[17] Recently, it has confirmed that CeO_2/C possesses an excellent ability for hydrogen peroxide electrosynthesis.[18] Whereas MnO_x are highly catalytically active towards the peroxide decomposition or disproponation reaction according to the previous literature,[8] thus one can expect an enhanced ORR performance when combined CeO_2 with MnO_x if the diffusion lengths is small and mass transfer rapidly. Therefore, we develop a novel strategy to combine MnO_x with CeO_2 nanoparticles in close proximity on low cost commercial conductive ketjenblack carbon (KB) with the aim of providing synergistic effects to enhance the ORR process of MnO_x. It is interesting to note that the ORR performance of the MnO_x-CeO_2/KB hybrid is on par with the commercial Pt/C. More importantly, the low cost MnO_x-CeO_2/KB hybrid shows a remarkable stability in alkaline solution, which is attractive for practical large-scale commercial applications.

The fabrication process of the MnO_x-CeO_2/KB hybrid can be described as a two-step strategy. Firstly, the KB

was dispersed into the $Ce(NO_3)_3$ solution and then CeO_2 nanoparticles were uniformly dispersed on the KB matrix after a facile hydrothermal process. Secondly, MnO_x particles were deposited on CeO_2/KB via the sacrificial oxidation of carbon in the presence of potassium permanganate, then the MnO_x-CeO_2/KB hybrid could be obtained by a simple heat treatment in inert gas. The structure and morphology of as-prepared MnO_x-CeO_2/KB hybrid were investigated by means of X-ray diffraction (XRD) and transmission electron microscopy (TEM), respectively. The XRD patterns of as-prepared samples are shown in Fig. 1. The XRD pattern of CeO_2/KB can be

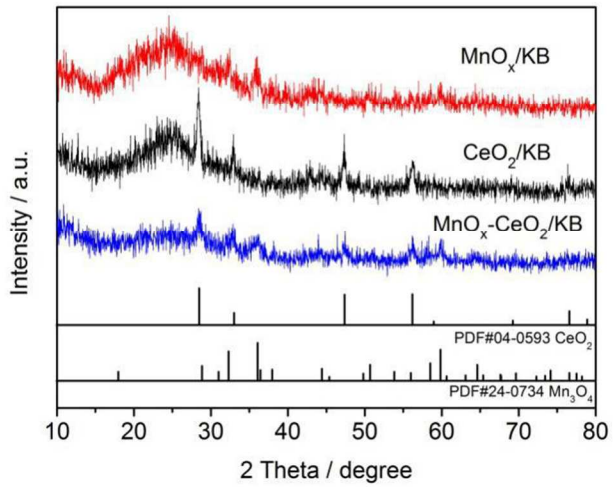

Fig. 1 XRD patterns of the MnO_x/KB, CeO_2/KB and MnO_x-CeO_2/KB.

well indexed to CeO_2 (JCPDS no. 04-0593) and the characteristic diffraction peaks of MnO_x/KB match those of Mn_3O_4 (JCPDS no. 24-0734). All of these characteristic diffraction peaks can be observed in the case of MnO_x-CeO_2/KB, which confirms the coexistence of CeO_2 and Mn_3O_4 in the hybrid. Good dispersion of MnO_x-CeO_2/KB particles is demonstrated in SEM images (Fig. S1, ESI†). High resolution TEM characterization (HRTEM) confirms

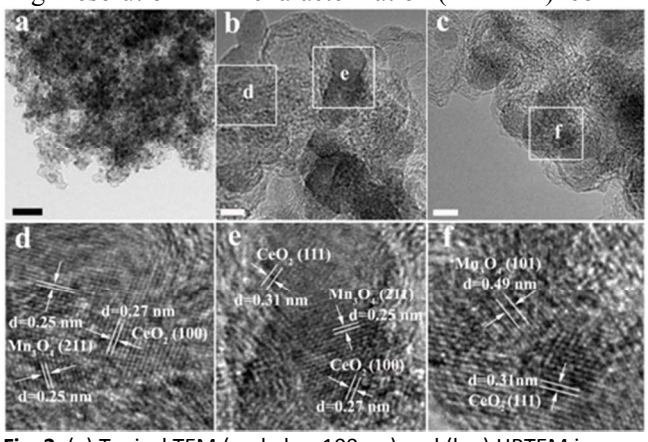

Fig. 2 (a) Typical TEM (scale bar 100nm) and (b-c) HRTEM images of the MnO_x-CeO_2/KB hybrid (scale bar 5 nm). (d-f) show the magnified HRTEM images for clearer lattice fringes in corresponding square region marked in (b) and (c).

the homogeneous distribution of nanosized CeO_2 and Mn_3O_4 with intimate contacted on the KB matrix identified by lattice analysis, in which the lattice spacing of 0.31 nm and 0.27 nm correspond to (111) and (100) planes of CeO_2, whereas the lattice spacing of 0.49 nm and 0.25 nm correspond to (101) and (211) planes of Mn_3O_4 (Fig. 2). Note that the particle sizes of CeO_2 and Mn_3O_4 are in 4-8 nm, which promises their intimate contact on the surface of KB carbon support, leading to better synergistic effect. Scanning TEM (STEM) and elemental mapping analysis of MnO_x-CeO_2/KB also proves the uniform distribution of the Mn, Ce and O elements throughout the carbon support (Fig. S2, ESI†). The metal oxides mass loading of MnO_x/KB and CeO_2/KB is about 22.6% and 14.6%, respectively, as determined by thermogravimertic analysis (TGA) result (Fig. S3, ESI†). The total mass loading of the MnO_x-CeO_2/KB hybrid is about 41.1%.

The chemical interaction of the various components of the MnO_x/KB, CeO_2/KB and MnO_x-CeO_2/KB hybrid were probed by X-ray photoelectron spectroscopy (Fig. S4, Fig. S5, ESI†). For the MnO_x-CeO_2/KB, the Mn 2p spectrum (Fig. S4a, ESI†) was deconvoluted into three different contributions at 641.0, 642.3, and 643.8 eV, which can be attributed to Mn^{2+}, Mn^{3+} and Mn^{4+} species, respectively.[19] The weak peak of Mn^{4+} indicates that the manganese is not phase pure but primarily consists of Mn_3O_4 based on the XRD and HRTEM results. For the case of the Ce 3d spectrum (Fig. S4b, ESI†), the peaks marked as u''', u'', u, v''', v'', and v are assigned to Ce^{4+}, whereas the peaks denoted as u' and v' are associated with Ce^{3+}.[20] The Ce 3d XPS spectra suggest the coexistence of Ce^{3+} and Ce^{4+} species but the Ce^{4+} is mainly valence state in MnO_x-CeO_2/KB catalyst as the peaks for Ce^{4+} is much stronger than that for Ce^{3+}. That is, $CeO_{2-\delta}$ is more appropriate for cerium oxide. The existence of Ce^{3+} could create a charge imbalance, the vacancies and unsaturated chemical bond, which will lead to the increase in chemisorbed oxygen.[20] The O 1s region was divided into three characteristic peaks at 530.2, 531.5, and 533.7 eV (Fig. S4c, ESI†). The sharp peak at binding energy of 530.2 eV is characteristic of lattice oxygen (denoted as O_α), the binding energy at 533.7 eV is due to oxygen-containing functional groups on the carbon surface (denoted as O_γ), and the energy at 531.5 eV is assigned to the chemisorbed oxygen species or the defect oxygen (denoted as O_β).[21]

In order to evaluate the electrocatalytic activities of as-prepared samples towards ORR, cyclic voltammogram (CV) curves were examined on a rotating disk electrode (RDE) in an O_2-saturated or Ar-saturated 0.1 M KOH solution. CV curves of as-prepared samples recorded in the Ar-saturated electrolyte show no obvious peaks. In contrast, when the electrolyte was saturated with O_2, a well-defined cathodic peak clearly appears, confirming the electrocatalytic activity for ORR. As seen in Fig. 3a,

MnO_x-CeO_2/KB shows an ORR onset potential of ~0.94 V (vs. RHE), which are much more positive than those for

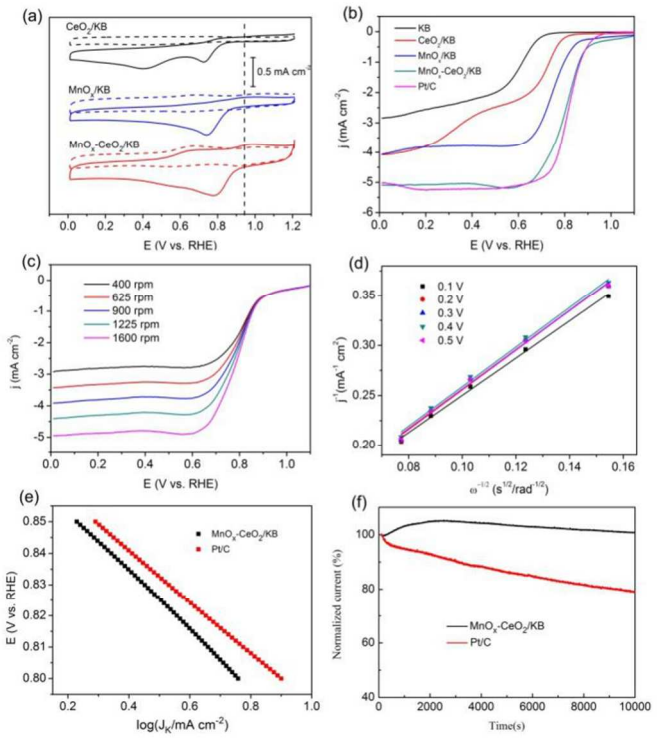

Fig. 3 (a) CVs of MnO_x/KB, CeO_2/KB, and MnO_x-CeO_2/KB in Ar- (dash) and O_2-(solid) saturated 0.1M KOH solution. (b) ORR polarization curves for each catalyst at 1600 rpm. (c) ORR polarization curves of MnO_x-CeO_2/KB at different rotating speeds. (d) K-L plots of MnO_x-CeO_2/KB at different potentials. (e) Tafel plots of of kinetic current for MnO_x-CeO_2/KB and Pt/C. (f) Current-time (i-t) chrono-amperometric response of MnO_x-CeO_2/KB and Pt/C at 0.7 V in O_2-saturated 0.1 M KOH.

CeO_2/KB (~0.82 V) and MnO_x/KB (~0.84 V). To obtain further insight into the ORR performance of each catalyst, the linear sweeping voltammograms (LSVs) at 1600 rpm in O_2-saturated 0.1 M KOH recorded on RDE are compared in Fig. 3b. All samples were scanned cathodically at a rate of 10 mV s^{-1}. The polarization curves show that the pure KB exhibits very low ORR activity. Two plateaus (form 0.8 to 0.5 V and from 0.5 to 0 V) are observed for CeO_2/KB, indicating that CeO_2/KB undergoes a two-electron pathway and proceeds via a hydroperoxide anion (HO_2^-) intermediate. MnO_x-CeO_2/KB has a more positive onset potential and higher limiting current density than those of CeO_2/KB and MnO_x/KB. The half-wave potential ($E_{1/2}$) of MnO_x-CeO_2/KB hybrid is 0.81 V, which is more positive than those of CeO_2/KB (0.67 V), MnO_x/KB (0.74 V), and only 10 mV negative shift compared with the commercial Pt/C catalyst (20 wt% Pt, Johnson Matthey). For comparison, the half-wave potential of MnO_x-CeO_2/KB here is more positive than that of most MnO_x-based electrocatalysts reported previously (typically less than 0.80 V),[4-7, 9-11, 22-24] highlighting the superior electrocatalytic activity of the MnO_x-CeO_2/KB hybrid for ORR.

To obtain further information about ORR kinetics, the Koutecky–Levich plots (j^{-1} vs. $\omega^{-1/2}$) of each catalyst are obtained from LSVs at various potentials. All plots show good linearity (R^2>0.99) at various rotation speeds (Fig. 3d, Fig. S7, ESI†). The electron transfer number (n) of KB was calculated to be 1.97, indicating that KB goes through a totally 2 electron transfer pathway. The n values for MnO_x-CeO_2/KB and Pt/C were calculated to be ~ 4 at a large potential range, which suggests a four-electron pathway for oxygen reduction. In contrast, the n values for CeO_2/KB and MnO_x/KB are 3.21 and 3.58, respectively, indicating the existence of a 2 electron reaction toward the formation of peroxide species (HO_2^-). The kinetic mass activity of the MnO_x-CeO_2/KB hybrid at 0.8 V is 71.7 A g^{-1}, which is much larger than those of CeO_2/KB (2.6 A g^{-1}), MnO_x/KB (15.8 A g^{-1}) and close to the value of commercial Pt/C (97.6 A g^{-1}). The Tafel plots of MnO_x-CeO_2/KB and Pt/C derived from LSVs data are shown in Fig. 3e, the Tafel slope of MnO_x-CeO_2/KB is 94.4 mV/decade, which is close to the 82.8 mV/decade of the Pt/C, indicating that the MnO_x-CeO_2/KB has a good kinetic process for ORR.

On the basis of experimental result of the larger limiting current density, more positive onset potential and increased electron transfer number of MnO_x-CeO_2/KB compared with the CeO_2/KB and MnO_x/KB. It is reasonable to conclude that there is a synergistic effect between CeO_2 and MnO_x towards ORR process. It should be noted that the Brunaer-Emmet-Taller (BET) surface area of the MnO_x/KB (411.1 m^2/g) and CeO_2/KB (429.4 m^2/g) are much higher than that of the MnO_x-CeO_2/KB hybrid (220.4 m^2/g), however, the MnO_x-CeO_2/KB hybrid with lower BET surface area shows a better ORR activity than those of MnO_x/KB and CeO_2/KB with higher BET surface area, indicating that more active sites may form at the interfaces of MnO_x and CeO_2 nanoparticles where an effective ORR would occur. Many reports have demonstrated that CeO_2 has the excellent ability of oxygen storage and oxygen release associated with its abundant oxygen vacancies and the ability of cerium ion to switch between the Ce^{4+} and Ce^{3+} as follows:[25]

$$CeO_2 \Leftrightarrow CeO_{2-x} + \frac{x}{2}O_2 \quad (0 \le x \le 0.5)$$

Thus the CeO_2 acts as an oxygen buffer and increases the local oxygen concentration of the catalyst. It can store O_2 during an oxygen-rich condition and remove it under lean conditions.[26] Therefore, it is reasonable to expect that when the O_2 partial pressure decrease, especially when oxygen concentration is low in the high current density region, the oxygen ions adsorbed on Ce^{3+} sites with oxygen vacancies and the HO_2^- intermediate at the surface of CeO_2 would be easily transferred to the adjacent MnO_x active sites. We believe that the fast supply of additional

oxygen and HO_2^- intermediate to the adjacent MnO_x could reduce the high overpotential and increased the electron transfer number, leading to an enhanced ORR performance.

To get a better understanding of the role of CeO_2 on the enhancement of catalytic activity for the ORR of MnO_x, the influence of CeO_2 loading on the catalytic performance of MnO_x-CeO_2/KB was also examined using the RDE (Fig. S8, ESI†). The different mass loading of CeO_2 in MnO_x-CeO_2/KB hybrid can be easily obtained by varying the concentration of the $Ce(NO_3)_3$ solution in hydrothermal process. It is found that only an appropriate ratio of CeO_2 gives the best ORR activity. The highest ORR activity is obtained at a CeO_2 mass loading of ~14.6%. More theoretical analysis and experimental characterizations are still necessary to unravel the detailed mechanism of ORR process of the MnO_x-CeO_2/KB hybrid.

Durability is another main challenge in real energy storage applications. The MnO_x-CeO_2/KB hybrid was also analyzed through chronoamperometric measurements at 0.7 V in O_2 saturated 0.1 M KOH. As revealed in current-time (i-t) curve (Fig. 3f), it seems that the MnO_x-CeO_2/KB goes through an activation process in the first 2000s as the current increases gradually and then decreases slowly. To the best of our knowledge, this phenomenon has never been reported in the previous literature. We believe that it may be due to the unique property of CeO_2, which could act as an oxygen buffer and feed the adjacent MnO_x with additional oxygen. The commercial Pt/C catalyst shows a current decrease (~80% retention) after 10000s. In contrast, the MnO_x-CeO_2/KB retains almost the same initial current, exhibiting an excellent stability in alkaline solution.

In summary, highly dispersed MnO_x-CeO_2/KB catalyst were successfully synthesized by a continuous two-step process. MnO_x and CeO_2 nanoparticles were uniformly dispersed on the KB matrix and CeO_2 nanoparticles can be found near MnO_x nanoparticles as seen from HRTEM. When CeO_2 nanoparticles are located in the vicinity of MnO_x nanoparticles, they might facilitate oxygen transfer to MnO_x nanoparticles, resulting in much better ORR activity. The low cost MnO_x-CeO_2/KB hybrid shows comparable ORR activity and much higher durability to the commercial Pt/C, which may provide a potential solution to the commercial ORR catalyst alternatives. The unique property of CeO_2 might also be applied to other ORR catalysts when designed properly.

This research was financially supported by the National Nature Science Foundation of China (No.21271187 and 21301193), Special Funded Project of the Postdoctoral Science Foundation of China (No. 2014T70781), the Opening Project of State Key Laboratory of Powder Metallurgy.

Notes and references

[a] *College of Chemistry and Chemical Engineering, Central South University, Changsha, 410083, P.R. China.*
E-mail: wanghy419@126.com; ygtang@csu.edu.cn. Tel.: +86 0731 8830886; fax: +86 0731 8879616.
[b] *College of Science, Hunan Agricultural University, Changsha, 410128, P.R. China.*
[c] *State Key Laboratory for Powder Metallurgy, Central South University, Changsha 410083, China*

†Electronic Supplementary Information (ESI) available: Details of the experimental section and supporting figures. See DOI: 10.1039/c000000x/

1. Z.-L. Wang, D. Xu, J.-J. Xu and X.-B. Zhang, *Chem. Soc. Rev.*, 2014, **43**, 7746-7786.
2. H. Zhang, H. Qiao, H. Wang, N. Zhou, J. Chen, Y. Tang, J. Li and C. Huang, *Nanoscale*, 2014, **6**, 10235-10242.
3. M. K. Debe, *Nature*, 2012, **486**, 43-51.
4. Y. Meng, W. Song, H. Huang, Z. Ren, S.-Y. Chen and S. L. Suib, *Journal of the American Chemical Society*, 2014, **136**, 11452-11464.
5. J.-S. Lee, T. Lee, H.-K. Song, J. Cho and B.-S. Kim, *Energy & Environmental Science*, 2011, **4**, 4148.
6. X. Lv, W. Lv, W. Wei, X. Zheng, C. Zhang, L. Zhi and Q. H. Yang, *Chemical Communications*, 2015, **51**, 3911-3914.
7. F. Cheng, T. Zhang, Y. Zhang, J. Du, X. Han and J. Chen, *Angewandte Chemie*, 2013, **52**, 2474-2477.
8. F. Y. Cheng, Y. Su, J. Liang, Z. L. Tao and J. Chen, *Chemistry of Materials*, 2010, **22**, 898-905.
9. J. S. Lee, G. S. Park, H. I. Lee, S. T. Kim, R. Cao, M. Liu and J. Cho, *Nano Letters*, 2011, **11**, 5362-5366.
10. D. J. Davis, T. N. Lambert, J. A. Vigil, M. A. Rodriguez, M. T. Brumbach, E. N. Coker and S. J. Limmer, *The Journal of Physical Chemistry C*, 2014, **118**, 17342-17350.
11. J. Duan, Y. Zheng, S. Chen, Y. Tang, M. Jaroniec and S. Qiao, *Chemical Communications*, 2013, **49**, 7705-7707.
12. I. Roche, E. Chaînet, M. Chatenet and J. Vondrák, *Journal of Applied Electrochemistry*, 2008, **38**, 1195-1201.
13. Z. Yan, J. Wang, R. Zou, L. Liu, Z. Zhang and X. Wang, *Energy & Fuels*, 2012, **26**, 5879-5886.
14. G. Chen, F. Rosei and D. Ma, *Advanced Functional Materials*, 2012, **22**, 3914-3920.
15. D. Zhang, L. Zhang, L. Shi, C. Fang, H. Li, R. Gao, L. Huang and J. Zhang, *Nanoscale*, 2013, **5**, 1127-1136.
16. Y. Tang, H. Qiao, H. Wang and P. Tao, *Journal of Materials Chemistry A*, 2013, **1**, 12512-12518.
17. H. T. Chung, J. H. Won and P. Zelenay, *Nature Communications*, 2013, **4**, 1922.
18. M. H. M. T. Assumpção, A. Moraes, R. F. B. De Souza, M. L. Calegaro, M. R. V. Lanza, E. R. Leite, M. A. L. Cordeiro, P. Hammer and M. C. Santos, *Electrochimica Acta*, 2013, **111**, 339-343.
19. Z. Liu, J. Zhu, J. Li, L. Ma and S. I. Woo, *ACS Applied Materials & Interfaces*, 2014, **6**, 14500-14508.
20. Y. Wang, C. Ge, L. Zhan, C. Li, W. Qiao and L. Ling, *Industrial & Engineering Chemistry Research*, 2012, **51**, 11667-11673.
21. J. Masa, W. Xia, I. Sinev, A. Zhao, Z. Sun, S. Grutzke, P. Weide, M. Muhler and W. Schuhmann, *Angewandte Chemie*, 2014, **53**, 8508-8512.
22. Y. Gorlin, C.-J. Chung, D. Nordlund, B. M. Clemens and T. F. Jaramillo, *ACS Catalysis*, 2012, **2**, 2687-2694.
23. Y. Gorlin and T. F. Jaramillo, *Journal of the American Chemical Society*, 2010, **132**, 13612-13614.
24. J. Zhang, C. Guo, L. Zhang and C. M. Li, *Chemical Communications*, 2013, **49**, 6334-6336.
25. G. Balducci, M. S. Islam, J. Kašpar, P. Fornasiero and M. Graziani, *Chemistry of Materials*, 2000, **12**, 677-681.
26. C. Sun, H. Li and L. Chen, *Energy & Environmental Science*, 2012, **5**, 8475-8505.

